A Physical Approach to Define a Class A Surface in Polymer Thermosetting Composite Materials

N. Boyard,[1] C. Serré,[2] M. Vayer[2]

[1]*Laboratoire de Thermocinétique de Nantes, UMR 6607 CNRS—Université de Nantes, La Chantrerie, rue Christian Pauc, BP 50609, F-44306 Nantes cedex 3, France*
[2]*Centre de Recherche sur la Matière Divisée, UMR 6619 CNRS—Université d'Orléans 1b, rue de la Férollerie, F-45071 Orléans cedex 2, France*

Received 18 April 2006; accepted 1 June 2006
DOI 10.1002/app.24927
Published online in Wiley InterScience (www.interscience.wiley.com).

ABSTRACT: In polymeric composite material, a class A surface is a high-quality surface according to its visual appearance. Bulk molding compound polymeric composites behave as a dielectric material with high bulk light scattering, low specular reflection, and low surface scattering. Gloss, related to specular reflection, is then low and cannot be a sufficient criterion to qualify a composite surface. For this purpose, we propose using either haze or roughness and power spectrum density (PSD) measured by AFM. An alternative solution to qualify a surface sample is to cover the sample by a metallic film. The sample then behaves as a metallic material with a main specular reflection and light scattering exclusively because of the surface. Measurements of gloss, haze, PSD, or roughness over a given spatial frequency range can qualify a sample surface and could especially define a surface in the class A family. © 2006 Wiley Periodicals, Inc. J Appl Polym Sci 103: 451–461, 2007

Key words: thermosets; atomic force microscopy (AFM); composites; surfaces

INTRODUCTION

Polymeric materials have grown in importance in the automotive industry. Polymeric materials have some significant properties that make their use as polymers and polymer composites advantageous over conventional metallic materials. They enable reduced weight, and, furthermore, reduced costs. Surface quality, however, has limited their application for exterior parts. Until now, polymer composites have rarely been used as visible parts in the production of automotive exteriors. To develop reinforced polymer composites for use in this field, high surface quality is needed.

Bulk molding compounds (BMCs) are widely used in the automotive industry thanks to their ability to produce a good surface finish and dimensional stability. To achieve these results, a thermoplastic additive [usually a low-profile additive (LPA)] is added to the thermosetting resin [generally composed of unsaturated polyester (UP) and styrene (ST)] in order to compensate for the high crosslinking shrinkage that occurs during the cure (between 7% and 10%[1–4]) by pore formation. Numerous experimental studies have sought to identify the mechanisms of crosslinking,[5–7] shrinkage compensation,[1,8–11] and microstructure formation.[2,12] It appears that the duration of phase separation between the LPA and UP/ST phases, the LPA volume fraction, and the chemical nature of the are important factors for shrinkage compensation (quantity and size of pores)[10,13] and for the final microstructure.[2,10,11,14–19]

Concerning the surface, previous works[15,18,20,21] used scanning electron microscopy, X-ray photoelectron spectroscopy (XPS) analysis, and infrared spectroscopy to demonstrate that BMC surfaces are composed of a pure organic layer (thickness $\approx$ 100 nm) with a mold release agent. Mineral fillers are localized just below, and glass fibers are located deeper (more than 0.4 μm).

Few studies have tried to characterize composite surface aspect quality (by human eye, profilometer, glossmeter, or commercial devices like the laser optic reflected image analyzer Diffracto-D-sight®),[22,23] to identify representative parameters (singular defects, roughness, texture/topography, waviness, anomalous panel shape),[22] or to quantify those parameters (Ashland Index, roughness, or gloss values). Several authors investigated the influence of composite formulations[24,25] and molding conditions (flowing,[26] pressure, and temperature[23,27,28]) on surface quality using the types of devices mentioned above. From a practical point of view, the surface quality of a material is defined using two visual impression parameters, gloss and haze. The interaction between light and matter leads to absorption, reflection, and scattering. Gloss is related to the capacity of a material to

Correspondence to: N. Boyard (nicolas.boyard@univ-nantes.fr).

reflect light in the main direction of reflection (the specular one). The scattered light causes haze, and the surface has a milky appearance.[29] The sum of the specular intensity, the surface and bulk scattering intensities, and the absorbed intensity is a constant equal to the incident intensity, and all these components are related to each other.

The general standard used to define high surface quality is a class A surface. However, there is no standardized definition of a class A surface.[22] The only general definition is that a composite material has a class A surface if its optical appearance is identical to an adjacent steel panel.[22,30] We have discussed this definition and addressed the question of whether a metallic material can have the same optical properties as a composite material. Boylan and Castro[30] defined a class A surface as a perfectly polished, high-luster surface free of porosity and scratches of any kind. Note, however, that in other respects quantification of surface quality remains basic (the Ashland Index in the SMC industry or measurement of the standard deviation of the experimental points with respect to the profile centerline, for example[22,30]).

The aims of this study were: (1) to define the optical behavior of a BMC material and how light interacts with the material and (2) to quantify the main components resulting from this interaction (absorption, reflection, and surface and bulk scattering). To our knowledge, studies of the optical properties of molded composite materials have been rarely reported in the literature. The two mainly visual parameters (gloss and haze) were measured using both an industrial approach (a haze-glossmeter) and a spectrophotometer and linked to topographic and optical characteristics. Moreover, a statistical tool was used to analyze the surface topography (power spectrum density), which was compared with these parameters. This led us to a novel approach in order to more fully define the quality of a class A surface of a composite material.

EXPERIMENTAL

Materials

The BMC composite materials were composed of (1) a polymeric thermoset blend (TB), (2) an internal mold release (calcium stearate, with a particle diameter ranging from 2 to 13 μm), (3) mineral fillers (calcium carbonate, with a particle diameter ranging from 1 to 10 μm), and (4) short glass fibers (12 μm in diameter and 3 mm long), some of which were ground. The TB was composed of (1) an unsaturated polyester prepolymer (UP), (2) a curing agent [styrene (ST)], (3) a polymerization initiator (tertiobutyl 2-ethyl perhexanoate), (4) a thermoplastic additive (TP), and (5) 2,6-di-tert-butyl-para-cresol as inhibitor. The exact composition of the BMC cannot be disclosed because of its industrial nature. However, the characteristics of the UP and TP in the BMC-H and BMC-G formulations are listed in Table I. Numerous other compositions have been tested. Because BMC-H and BMC-G behaved typically, we focused on these two samples.

TABLE I
Chemical Characteristics of Thermosetting Resins and Thermoplastic Additives of BMC Materials Studied (All Supplied by DSM Composite Resin, Germany)

	Chemical nature of UP	Chemical nature of TP
BMC-H	P18-03 Maleic anhydride + propylene glycol + ethylene glycol	H892-02 Adipic acid + propylene glycol + ethylene glycol + neopentyl glycol
BMC-G	P174-01 Maleic anhydride + orthophtalic anhydride + cyclopentadiene	8199-M1 Poly(methyl methacrylate)

BMC plates (120 × 250 × 3 mm) were molded by compression using a Derek press in a stainless-steel mold. Special attention was paid to the level of polishing of the female part of the mold because the topography of the composite panel depends on the topography of the molding print. The arithmetic roughness of the mold, R_a, was 5 nm. The female part was heated at 150°C and the punching die at 135°C. Pressure applied on the material was 10 MPa, and curing time was 100 s.

Some plates were also metallized with aluminum using a chemical vapor deposition (CVD) process. The thickness of the aluminum layer was determined to be 100 nm. This treatment allowed the topography of the surface to be replicated and a metallic surface to be obtained.

Instrumentation

Spectrophotometer

Scattering reflectance and total reflectance were measured using a Lambda-900 spectrophotometer from Perkin–Elmer, equipped with an integrating sphere. Measurements were performed at every 10th nanometer for wavelengths between 380 and 780 nm. The diameter of the integrating sphere was 15 cm.

Haze-glossmeter

The gloss and haze properties of the plates were determined according to ASTM method D 523 using a haze-gloss tester (Byk-Gardner, Silver Spring, MD). A test measurement was performed with 60° geometry, that is, the light source impinged the sample surface with an incident angle of 60°/normal. A detector recording the gloss (G) values was placed in the spec-

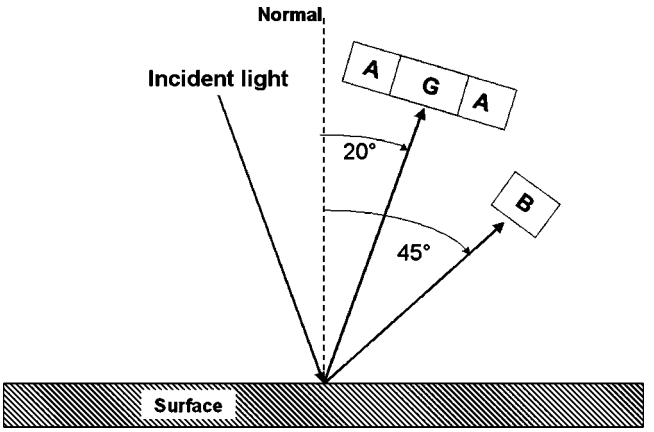

Figure 1 Description of the detectors positions in the haze-glossmeter [A, total scattering; B, bulk scattering; G, gloss (specular reflectance)].

ular position (−60°/normal) with an aperture of 1.8°. According to the ASTM method, because almost all the surface samples had a gloss value higher than 70 gloss units, the samples were characterized has having high-gloss surfaces, and measurements were performed with a 20° geometry. Two additional detectors were positioned on each side of the gloss measurement detector (Fig. 1). The measured value denoted as A represented the total scattering of the material (i.e., the sum of the surface scattering and the bulk scattering, as explained later). Another detector was placed 25° out of the specular direction (i.e., 45°/normal), and its measured value, denoted as B, was representative of the bulk scattering (more precisely, B was only a small part of the total bulk scattering). Because A and B were measured over the same angular aperture, it was possible to determine the haze, H (in arbitrary units, U), which was related to the surface scattering reflectance, equal to $(A - B)$. The relation between the haze and the surface reflectance was a logarithmic relationship[29] provided by the manufacturer of the haze-gloss tester, taking into account its geometric configuration:

$$H = 1285.1^{*} \log\left[\frac{A-B}{20} + 1\right] \quad (1)$$

Polished black glass with a refractive index of 1.567 was used to calibrate the gloss. The absorbance coefficient of the standard was assumed to be zero, and the gloss of this glass was arbitrarily set to 100 U and its reflectance (given by the Fresnel equation) was near 5%. Consequently, incident light intensity was then evaluated to 2000 U.

Atomic force microscopy

Atomic force microscopy (AFM), which enables the topography of a surface to be defined, was carried out in air using Nanoscope III from Digital Instrument Corporation in the contact mode. The piezo scanner was able to scan with a horizontal range of 150 μm and a vertical range of 7 μm. Microfabricated Si_3N_4 gold-coated cantilevers, 250 μm in length, with integrated Si_3N_4 pyramidal tips were used. The spring constant of the cantilevers was 0.06 N/m. The theoretical lateral resolution was 1 nm. The images were constituted by N × N = 512 × 512 pixels. The typical size of a BMC sample studied with AFM was around 1 cm^2. For a commodity, we denoted L as X μm for images $X \times X$ μm^2 in size.

Theoretical background

Topography of a surface

The topography of a surface is theoretically defined by its amplitude, z, as a function of x and y, that is, $z(x,y)$.[31] From an analytical point of view, a surface could be defined by $z(m,n)$. If x and y range between 0 and L_x or L_y, m and n range between 0 and $(N - 1)$. The space step is then $\Delta x = L_x/N$ and $\Delta y = L_y/N$.[30]

The topography of a surface can be characterized by its roughness, which has several definitions.[32] Themost commonly used are root-mean-square roughness (R_{rms}) and arithmetic roughness (R_a), expressed as[33]

$$R_{rms} = \left[\frac{1}{L_x L_y}\int_0^{L_x}\int_0^{L_y}(z(x,y) - \bar{z})^2 dxdy\right]^{1/2} \quad (2)$$

$$R_a = \frac{1}{L_x L_y}\int_0^{L_x}\int_0^{L_y}|z(x,y) - \bar{z}|dxdy \quad (3)$$

where $\bar{z}$ is the average amplitude and L_x and L_y are the size of the image along the x and y axes, respectively.

Statistical functions were used to describe the surface topography more deeply. The power spectrum density (PSD) allowed us to obtain information on the distribution and periodicity of the roughness. The PSD S(ν) corresponds to the Fourier transform of the autocorrelation function of the surface.[31,34] It can also be defined as the square of the Fourier transform of the surface profile, $z(x,y)$:

$$S(\vec{\nu}) = \frac{1}{L_x L_y}\left[\int_{L_x}\int_{L_y} z(x,y) \times \exp(-2\pi j(\nu_x x + \nu_y y))dxdy\right]^2 \quad (4)$$

where ν_x and ν_y are the spatial frequencies in directions x and y and j is defined such that $j^2 = -1$.

The PSD can be defined as the roughness power per spatial frequency unit. The calculated PSD curve is symmetric with respect to the S(ν) axis.[31] For a commodity, the spatial frequencies on a PSD graph are generally only displayed with positive values.

The discrete PSD is expressed as

$$S_{pq} = S(p\Delta\nu_x, q\Delta\nu_y) \tag{5}$$

where $\Delta\nu_x$ is $1/L_x$, $\Delta\nu_y$ is $1/L_y$, $1/L_x \leq p\ \Delta\nu_x \leq N/2L_x$, and $1/L_y \leq q\ \Delta\nu_y \leq N/2L_y$, for p and q ranging from 1 to $N/2$. In AFM, L_x equals L_y equals L. The band of spatial frequency analyzed by AFM is then [$1/L$; N/2L].[34–37] For AFM images of 50 × 50 μm^2, the spatial frequency band is [0.02; 5.12] μm^{-1}.

PSD graphs are very useful for comparing surface topographies.[38–40] For example, a peak at a frequency of ν_p implied a surface structure with a periodicity of $1/\nu_p$. Moreover, the R_{rms} between two frequencies, ν_1 and ν_2 (named R_{rmsv} because it is proportional to the integration of the PSD between ν_1 and ν_2), can be calculated. PSD analysis enabled comparison of the roughness spectra of the samples.

The R_{rms}, defined in eq. (2), corresponds to the PSD integrated over the band of the spatial frequency analyzed by AFM and is then [$1/L$; N/2L].

Interaction between light and a material

The interaction between matter and light leads to different phenomena (Fig. 2). The first part of an incident light beam is absorbed, a second part is transmitted, and the last part is reflected in all directions of space.

A reflected beam is composed of: (1) a specular component (it is reflected with an angle, θ_s, equal to the incident angle, θ_i) whose intensity is a function of the refractive index according to the Fresnel equation and (2) a scattered component corresponding to scattering in all directions of space. From this the surface scattering induced by irregularities in the surface and bulk scattering due to bulk inhomogeneities of the refractive index can then be distinguished.[41,42] A previous study demonstrated that surface light scattering occurs around the specular reflection beam, whereas light scattered by the bulk is spread over space in all directions.[43]

For a metallic surface, there is no light bulk scattering.[44] Specular intensity can be approximated by the following equation:[31,45,46]

$$\frac{I_{specular}}{I_{total}} = \exp\left[\left(\frac{4\pi \times R_{rms} \times \cos\theta_i}{\lambda} \right)^2 \right] \tag{6}$$

where $I_{total} = I_{specular} + I_{surface\ scattering}$ and λ is the wavelength of the incident light.

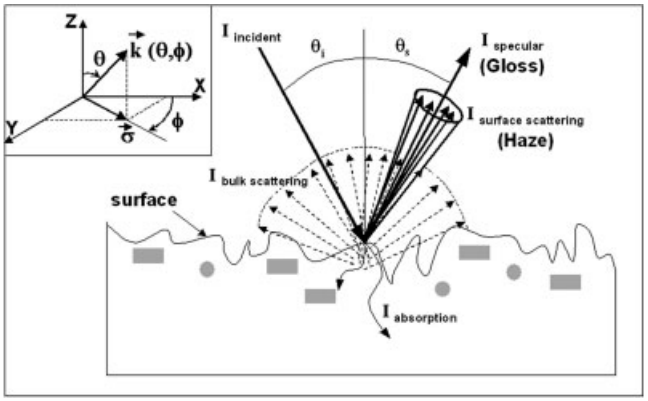

Figure 2 Interaction between the light and a material [inset: a scheme describing the vectors and angles used in eqs. (8) and (9)].

Specular and surface scattering intensities depend on the roughness of the surface. It is possible to distinguish two main cases.

(1) The roughness of the surface is low compared to the wavelength of the incident light (i.e., $R_{rms} < 0.05\lambda$). $I_{specular}$ then nearly equals the total reflection intensity. Consequently, the scattering intensity ($I_{surface\ scattering}$) is very low compared to $I_{specular}$, and it is possible to write eq. (6) as

$$\frac{I_{surface\ scattering}}{I_{total}} \approx \left(\frac{4\pi \times Rms \times \cos\theta_i}{\lambda} \right)^2 \tag{7}$$

This is called the total integrated scattering (TIS) ratio.[38,39,47]

Furthermore, for surfaces with low roughness and for a scattering vector, $\vec{k}$, equal to ($\vec{k}_s - \vec{k}_i$) where $\vec{k}_s$ is the scattering light vector and $\vec{k}_i$ is the incident light vector, $I_{surface\ scattering}$ is also expressed as[38,39,41,46,48]

$$I_{surface\ scattering} = C(\theta, \phi) \times S(\vec{\sigma}) \tag{8}$$

where C is an optical factor coming from the electromagnetic theory, S is the PSD, $\vec{\sigma}$ is spatial pulsation, projection of $\vec{k}$ on the surface, θ is the angle between the scattering vector, $\vec{k}$, and the normal and ϕ (azimuth) is the angle between the x axis and $\vec{\sigma}$. The vectors and angles are shown in the inset in Figure 2. The components along the x and y axes of $\vec{\sigma}$ could be written as

$$\sigma_x = \frac{2\pi}{\lambda}\sin\theta\cos\phi \quad \text{and} \quad \sigma_y = \frac{2\pi}{\lambda}\sin\theta\sin\phi \tag{9}$$

Eq. (8) shows that light surface scattering (with a wavelength, λ) is directly related to the PSD of the surface. The roughness frequency window ($\nu = \sigma/2\pi$) explored by light scattering is clearly defined. It is a function of the wavelength and the probed angular domain.

In the peculiar case of the haze-glossmeter, the incident angle is 20° with respect to the normal, and the light-scattering measurements were carried out between 17.3° and 22.7° with a white light beam ($300 < \lambda < 800$ nm) and the incident light and the detector in the same plane ($\phi = 0$). The optical window is determined as follows for the x direction:[35]

$$[\nu_{min}; \nu_{max}] = \left[\frac{\sin\theta_i + \sin\theta_s}{\lambda_{max}}; \frac{\sin\theta_i + \sin\theta_s}{\lambda_{min}}\right] \quad (10)$$

where θ_i and θ_s are the incident and scattering angles, respectively, and λ is the wavelength of the light. The spatial roughness frequencies scanned with the haze-glossmeter thus ranged between 0.8 μm^{-1} ($\theta_i = 20°$, $\theta_s = 17.3°$, $\lambda_{max} = 800$ nm) and 2.4 μm^{-1} ($\theta_i = 20°$, $\theta_s = 22.7°$, $\lambda_{min} = 300$ nm). Human eyes can scan a larger frequency range: between 0.09 μm^{-1} ($\theta_i = \theta_s = 2°$, $\lambda_{max} = 800$ nm) and 6.66 μm^{-1} ($\theta_i = \theta_s = 88°$, $\lambda_{min} = 300$ nm), if a scanning incident and scattering angles ranging between 2° and 88° are considered. This range is comparable to those scanned with an AFM image of 50 × 50 μm^2, ([0.02; 5.12] μm^{-1}, as calculated above).

(2) For surfaces with a higher roughness, the scattering intensity is close to I_{total}. The specular intensity can be then approximated by the following equation:

$$I_{specular} \approx \exp(-R_{rms}^2) \quad (11)$$

However, the roughness frequency band, larger than in the previous case, is difficult to define.[46] Note that a rough surface has a large effect on the amount of light that is specularly reflected from that surface.[49]

These relationships can only be applied to metallic systems. No relationship has been proposed for dielectric material, for which bulk scattering is not negligible.

RESULTS AND DISCUSSION

Study of surface aspects by AFM analysis

Reproducibility of roughness and PSD measurements

The roughness, measured as R_a and R_{rms} over a scanned area of 150 μm, of all the BMC raw samples in this study was less than 40 and 60 nm, respectively.

A preliminary study was performed to determine the influence of the size of the scanned area for a typical BMC sample. Images of increasing size of a typical BMC sample were recorded, and the roughness, R_a, was calculated using eq. (3) (reproducibility = 1%). R_a varied as a function of image size, as depicted in Figure 3. The roughness increased continuously up to an image dimension, L, of 20 μm and remained constant

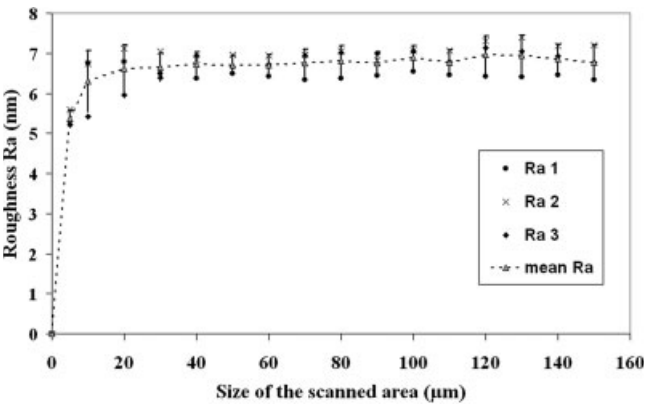

Figure 3 Reproducibility of the roughness (R_a) measurement as a function of the scanned size by AFM.

(average $R_a = 7.1$ nm, standard deviation = 0.7 nm) beyond that. The measurements were performed in three places on the plates and exhibited good reproducibility (identical PSD spectra). This confirmed the homogeneity of the molded plates.

The PSD spectra were calculated for images of different sizes. Figure 4 presents the PSDs for 3 sizes, L = 10, 100, and 150 μm. The spectra were superimposed in the shared frequency ranges, demonstrating that the data obtained with the AFM were reliable.[36,44] We were then able to perform a multiscale analysis of the roughness. Low spatial frequency corresponded to information on a microscopic scale, whereas high spatial frequency corresponded to information on a nanoscopic scale.

The reproducibility of the PSDs was also verified (the spectra are not displayed here for simplification), which was 2%. PSD spectra of three different-sized areas of the same composite plate were calculated and compared (standard deviation = 4%). Because they were superimposed well, the PSDs were independent of the area studied. This also confirmed the homogeneity of the molded plates.

Two BMCs (designated BMC-H and BMC-G), each exhibiting a typical behavior, were studied. BMC-H had low roughness ($R_{rms} = 14$ nm), whereas BMC-G had high roughness ($R_{rms} = 52$ nm). These R_{rms} values were obtained from AFM images $L = 50$ μm in size.

Influence of metallization process on the surface aspect

To differentiate surface from bulk scattering resulting from the heterogeneity of the refractive index of the material,[41,43,48] the samples were coated with aluminum (thickness ≈ 100 nm). The basis for performing this treatment was the strong hypothesis that it did not modify the initial roughness of the surface (i.e., before metallization).[41,48,50–52] Thus, we obtained a

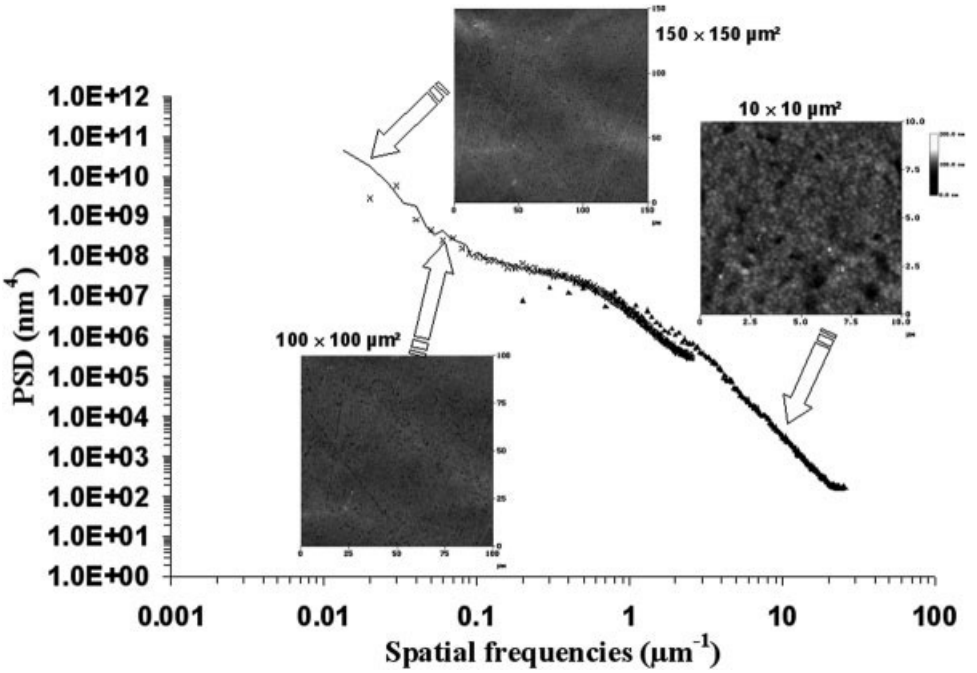

Figure 4 PSD spectrum as a function of size of the scanned area (L = 150, 100, and 10 µm).

metallic surface with negligible bulk scattering (thanks to its refractive index[42]). AFM images of raw and metallized surfaces of BMC-H and BMC-G were recorded. A comparison of the shapes of the PSD spectra of raw and metallized surfaces of BMC-H and BMC-G formulations (Fig. 5) demonstrated that the metal coating reproduced the raw surface of the sample. However, the variation in PSD values (up to ≈ 40%) indicated that the roughness was slightly modified, as shown in Table II.

Roughness and PSD results

All the BMCs were molded in the same experimental conditions. Figure 6(a,b) displays the surface morphologies of BMC-G and BMC-H, respectively, characterized by AFM on a microscopic scale (image size: L = 150 µm). Summarized in Table II are the surface roughness values computed using eqs. (2) and (3) (arithmetic and root mean square), determined for an image size of L = 50 µm. For each BMC formulation, surface roughness was calculated as the average of the values obtained from 20 images derived from two different BMC samples.

The BMC-H sample exhibited a smooth surface (R_{rms} = 14 nm) without any apparent defect. The white lines shown in Figure 6(b) corresponded to small polishing stripes. However, BMC-G was found to have higher roughness with many cracks (R_{rms} = 52 nm). The presence of cracks or holes was responsible for the increase in the global roughness. A previous study[21] demonstrated that the BMC surfaces were constituted by a pure organic surface layer (thickness ≈ 100 nm). This layer exhibited small particles linked together in aggregates (around 300 nm in

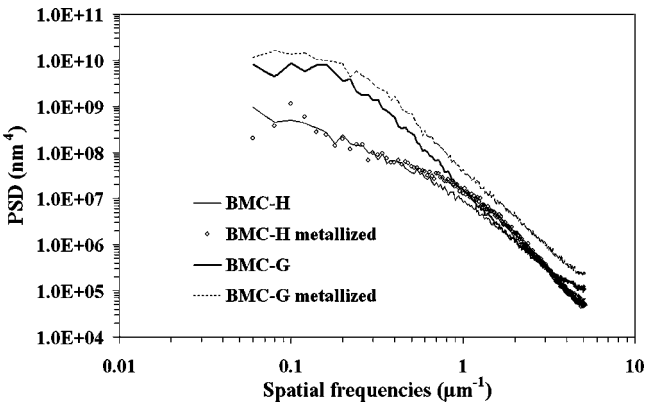

Figure 5 PSD spectra of BMC-H and BMC-G samples before and after metallization (L = 150 µm).

TABLE II
R_a, R_{rms}, and R_{rmsv} Values for Surfaces of BMC-G and BMC-H and Corresponding Metallized Samples

Sample	R_a (nm)	R_{rms} (nm)	R_{rmsv} (nm)
BMC-G	37 (± 10)	52	8.3
BMC-H	10 (± 2)	14	6.9
BMC-GM	41 (± 9)	56	9.1
BMC-HM	13 (± 3)	19	7.2

R_a and R_{rms} were calculated for the whole frequency range (size of AFM image: L = 50 µm), whereas R_{rmsv} was determined in the optical window of the haze-glossmeter [0.8; 2.4] µm^{-1}.

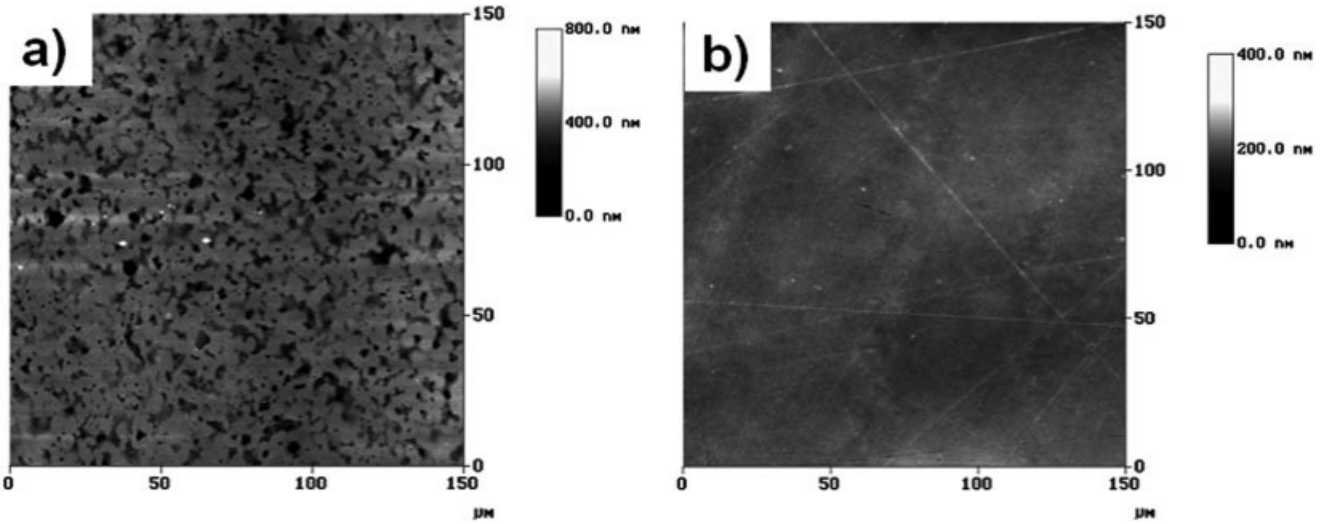

Figure 6 AFM images of the surfaces of (a) the BMC-G sample and (b) the BMC-H sample.

size). The topography of the surface was largely influenced by the compensation for shrinkage. When shrinkage compensation in the bulk was low (no pores formation and compact particles network), important stresses were generated throughout the sample, inducing strong surface deformations, which finally created cracks and/or holes (BMC-G). In contrast, when shrinkage was highly compensated, pores were formed in the bulk, allowing stress relaxation. There was then no surface deformation, and the surface was smooth (BMC-H).

The frequency range scanned by the human eye was [0.09; 6.66] μm^{-1}. It was thus interesting to have PSD spectra over the same frequency range. They were calculated for AFM images $L = 50$ µm in size (Fig. 7). The PSD spectrum of BMC-H indicated low roughness over the whole spatial frequency range compared to BMC-G. In contrast, the PSD of BMC-G shifted to higher values at low frequencies and exhibited a wide peak at approximately 0.1 μm^{-1} (corresponding to a characteristic distance of 10 µm). This peak was attributed to the distance between the holes observed on the AFM image. Such a PSD result showed that BMC-G had a worse surface aspect. As can be seen, PSD was an interesting tool for classifying surface quality of a composite material on various scales.

Characterization of optical and visual properties of BMC materials

As described above, during interaction between the light and a surface, one part of the light beam was reflected. This reflectance had a specular component and a scattered component (surface and bulk scattering).

We used spectrophotometry to measure total reflectance, absorbance, specular reflectance, and scattering reflectance as a function of incident light wavelength for an incident angle of 8°/normal. Three tests were performed on each sample. The standard deviation of the measurements was estimated as ±1%.

The total reflectance of BMC-H [Fig. 8(a)] was around 80% and varied slightly with incident wavelength. This was a result of the absorbance, mainly induced by the mineral part of the composite, which absorbed the light as a function of wavelength. Absorbance was then around 20%. Four percent of the reflectance was specular, and 76% was scattered (surface and bulk scattering).

The shape of the curves of the BMC-G sample (not displayed) was similar to that of the BMC-H sample. However, because the mineral part of the BMC-G composite was totally different from that of the BMC-H formulation, absorbance was not exactly the same, and the average total reflectance was slightly higher (87%), with a specular component of 3% and a scattered component of 84%.

Absorbance did not vary with incident wavelength for the metal-coated BMC samples (designated as

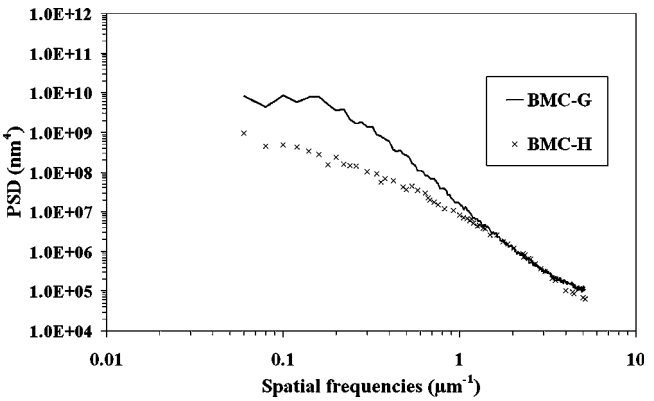

Figure 7 PSD spectra of BMC-G and BMC-H samples for an AFM image size of $L = 50$ µm.

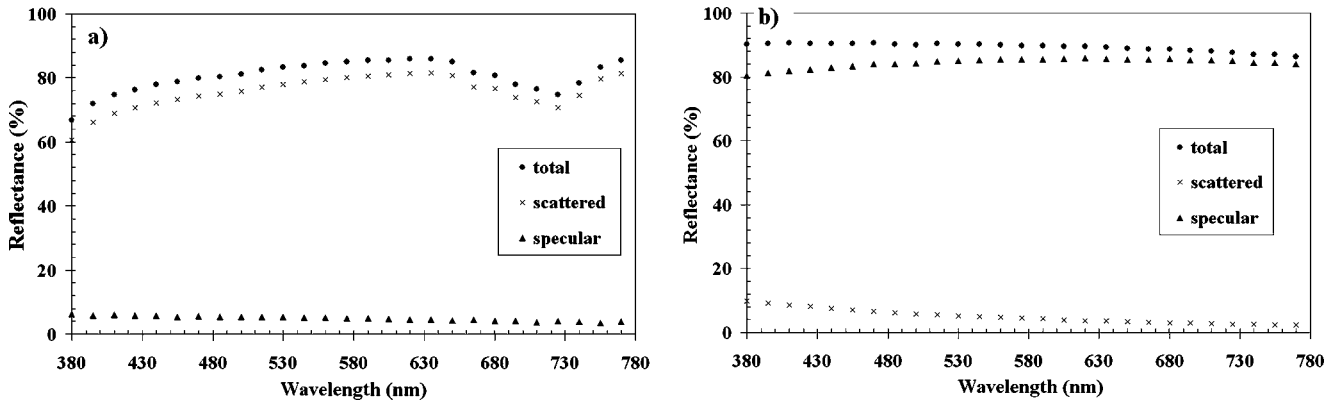

Figure 8 (a) Reflectance measurement versus wavelength for the (a) BMC-H sample surface and (b) BMC-HM sample surface (incident angle = 8°/normal).

BMC-HM and BMC-GM). Figure 8(b) shows the average total reflectance of BMC-HM was also around 90%, with the specular component approximately 85% but the scattering component only about 5%. For BMC-GM, the average total reflectance was 95%, which was subdivided as about 84% specular reflectance and about 12% scattering reflectance. These results demonstrated the influence of roughness on surface scattering.

Specular reflectance was measured with the spectrophotometer as a function of the incident angle of the light. The incident light beam had a wavelength, λ, of 633 nm and impinged the surface with a variable incident angle [Fig. 9(a,b)].

For the raw samples (i.e., without metal coating), specular reflectance first decreased very slowly, in the range of 10°–50° of the scattering angle, and then increased strongly from 60° regardless of the sample [Fig. 9(a)]. This behavior was characteristic of a dielectric material, in which light scattering results from both bulk scattering and surface scattering.[42]

In contrast, specular reflectance was constant for BMC-HM, whatever the incident angle [Fig. 9(b)]. This behavior was characteristic of a metallic material, in which light scattering results only from surface scattering and no bulk light scattering occurs.

With the assumption that a metal deposit only allowed a metallic surface with a topography exactly like that of a BMC sample, we decided that the surface light-scattering intensity of a metallic sample was the same as that of a raw sample. Thus, we concluded that the surface light scattering of a BMC was only 5% of the total light scattering. The main part of the scattering was bulk light scattering.

Finally, we used the spectrophotometer to measure scattering reflectance versus scattering angle. The incident light beam had a wavelength, λ, of 633 nm and impinged the surface with an incident angle of 20°/normal. The scattering angle ranged between 10° and 70° with respect to the specular reflection angle.

For the raw samples (Fig. 10), scattering reflectance decreased progressively when the scattering angle was in the range of 10°–50°. Scattering reflectance continued to decrease up to a scattering angle of 70° with respect to the specular beam. The shape of the curve followed a Lambertian law, where the scattering reflectance was proportional to the cosines of the scattering angle.[31,42,43,52,53] According to these results,

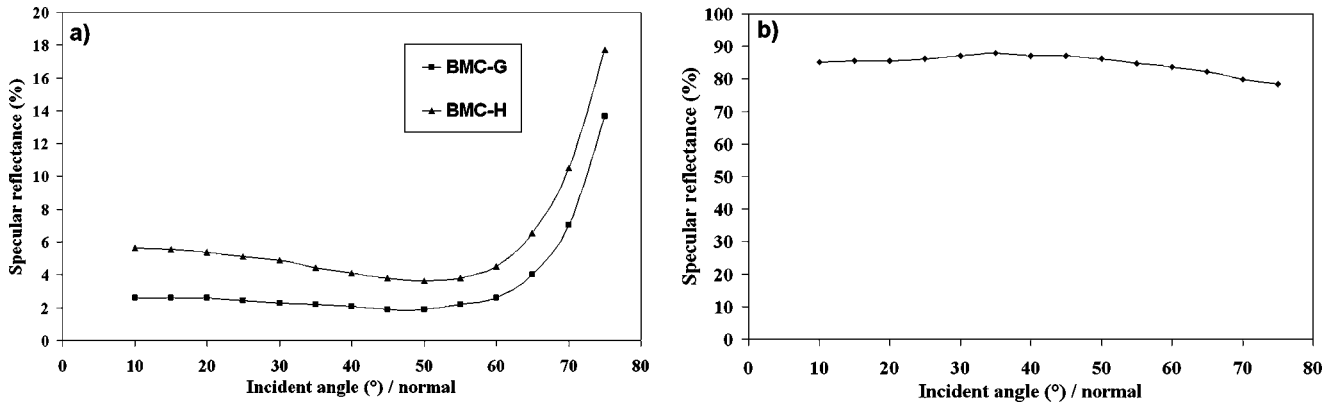

Figure 9 Specular reflectance versus incident angle for (a) BMC-G and BMC-H samples and (b) metal-coated BMC-HM sample (λ = 633 nm).

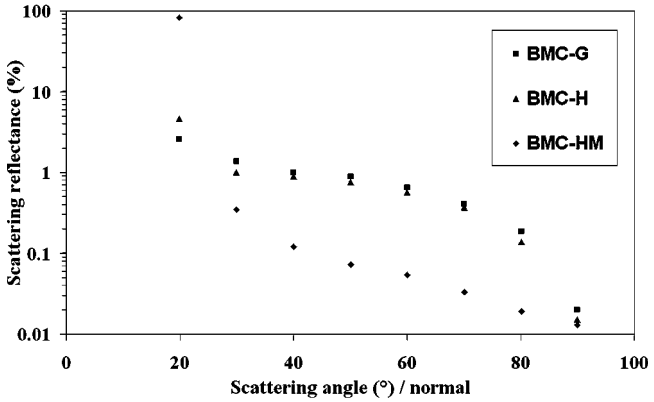

Figure 10 Angular scattering of the BMC surfaces studied ($\lambda = 633$ nm, incident angle $= 20^\circ$/normal).

such a model is typical of bulk light scattering and provides evidence that bulk scattering governed the scattering of the raw BMC samples. Figure 10 also highlights that the scattering reflections of the BMC-H and BMC-G samples were identical in terms of bulk scattering, despite having different roughness values ($R_{rms} = 14$ and 52 nm, respectively). The bulk scattering seemed to be remain constant whatever the BMC sample. As a BMC is a dielectric material, bulk scattering could not be avoided. Consequently a good surface aspect was characterized by a low surface scattering, that is, low roughness.

For the BMC-HM, scattering reflectance decreased progressively with scattering angle. This behavior was typical of a metallic sample.[42]

Surface quality study using haze-glossmeter

For bulk molded compound panels, the objective was to achieve good surface quality, that is, a high-gloss and low-scattering surface (haze). The gloss was mainly a function of material absorption and bulk and surface scattering. The volume and surface properties then had to be carefully considered. Only surface properties (roughness) were taken into account for the haze.

Samples were characterized with the haze-glossmeter, and the results (averages) are shown in Table III. Gloss measurements were reproducible within 1%, and the standard deviation of a whole composite panel did not exceed 4%. The haze results were more heterogeneous: reproducibility reached about 6%, and the standard deviation of the values for a BMC panel was 15%.

Gloss was between 600 and 1850 U for the metallized samples. This was also in good agreement with the spectrophotometric evaluation. Because there was no bulk scattering, haze was related to the surface scattering reflectance, suggesting that the haze enabled classification of the surface quality. This classification was also in agreenebt with the classification obtained using roughness determined by AFM. Moreover, for a metallized surface, light was reflected or scattered by the surface, and the refraction index was the same for all the samples, namely, the aluminum ones. Consequently, gloss or haze could be used to classify surface aspects of the samples. Moreover, becuase the gloss and haze values were high, it was possible to distinguish samples that were rather similar.

For the raw samples, gloss was less than 110 U. This value allowed specular reflectance (%) to be calculated and compared with that determined by spectrophotometry (Table III), which was found to be in good agreement. Haze (H) was a pertinent parameter for comparing the surface scattered reflectance of different BMCs. As is illustrated in Table III, the smaller the surface roughness, the smaller was the haze. Consideration of A and B and calculation of the percentages of surface and bulk scattering relative total scattering (Table IV) demonstrated again that bulk light scattering was the dominant phenomenon. Indeed A–B was never negligible compared to B. However, taking haze into consideration allowed samples to be compared and classified.

For raw samples with low surface roughness, surface scattering reflectance (A–B) determined by the haze-glossmeter [see eq. (1)] could be correlated with the roughness measurements from AFM in the same

TABLE III
Experimental Data Determined by Haze-Glossmeter

	Gloss (U)	Haze (U)	A (a.u.)	B (a.u.)	Specular reflectance (%)	Specular reflectance by spectrophotometry (%)
BMC-H	97 (4)	15 (3)	4.0	2.9	5	5
BMC-G	43 (5)	93 (9)	6.0	3.0	2	3
BMC-HM	1800 (65)	300 (25)	16	0	90	95
BMC-GM	715 (20)	690 (18)	50	0	35	40

Numbers in parentheses are standard deviations. Specular reflectance values calculated with a spectrophotometer are given for comparison. Haze gives an idea of the surface quality.

TABLE IV
Proportions of Surface and Bulk Scattering Reflectance with Respect to Total Scattering Intensity (Calculated from Haze-Glossmeter Measurements)

Sample	Surface scattering reflectance (%)	Bulk scattering reflectance (%)
BMC-G	50	50
BMC-H	27	73

frequency range (Fig. 11). Given that eq. (7) was valid for metallic surfaces with low roughness (R_{rms} was calculated for a given frequency range[34–37,39]), we were able to demonstrate a similar relation for BMC plates with several similar formulations and low roughness ($R_a < 10$ nm):

$$I_{\text{surface scattering}} = k(R^2_{\text{rmsv}}) \tag{12}$$

where k is a constant and R_{rmsv} is the roughness corresponding to the spatial frequencies scanned by the haze-glossmeter. This result confirmed interest in haze as a pertinent parameter for determining surface quality.

CONCLUSIONS

A reinforced thermoset composite is a dielectric material. Its specular reflectance, which gives the gloss of a surface, is less than 5%. The main part of the reflectance is bulk scattering (more than 70%), which depends on the bulk composition of the composite. The surface scattering reflectance, which is connected to the topography of the surface, represents less than 5% of the reflected light. This contribution depends on both composite composition and the material process, which of which affect the surface topography. These results demonstrated, of course, that a dielectric surface never behaves like a metallic surface. Consequently, it is not realistic to have the actual definition of a class A surface (see the Introduction section).

A class A surface cannot have a specular reflectance higher than 10% because of the dielectric nature of polymer composites. We have highlighted that surface properties (roughness, topography), which influence surface scattering, have to be carefully considered when surface aspects are studied. In addition, we found that surface quality could be classified in relation to its surface scattering reflectance. A high-quality or class A surface has low surface scattering reflectance. This quality can be evaluated by measuring the haze of the samples with a haze-glossmeter, for example. As surface scattering is correlated to surface topography, the quality of the surface also can be estimated by using AFM and determining roughness in the optical frequency range using PSD analysis. Haze, roughness, and PSD spectra gave the same sample classification. Moreover, for low roughness surface (R_a lower than 10 nm), haze was proportional to the squared R_{rms} taken over the same frequency range (i.e., R^2_{rmsv}). To decide if a sample had a class A surface, the haze or roughness value could be considered for raw samples and then compared to threshold values, which define a class A surface. These values remain to be defined by users.

Another solution for classifying samples can be to metallize the samples and explore their visual appearance. The samples then have a metallic behavior with a specular reflectance higher than 70% and a scattering reflectance only due to surface topography of less than 5%. Thus, gloss, haze, or roughness over the visual frequency band can be used to classify the samples. With these conditions, gloss, haze, or roughness can be considered for evaluating if a metallized sample has a class A surface. As previously mentioned, threshold values corresponding to a class A surface have to be estimated.

Finally, it appears that the PSDs calculated from AFM images were very convenient for performing a multiscale analysis of the material structure. Applied to BMC composite materials we highlighted that the surface aspect differed from a nanoscopic to a microscopic scale. From a practical point of view, a PSD representation of various composite surfaces was a simple and robust way to determine the best surface aspect of composite pieces. The lower the PSD, the better was the surface quality. In our opinion, by using the PSD of a mirror-polished metallic surface (low roughness) as a reference, we were able to determine that the quality of the surface of a composite material was class A when the PSD was close to that of the reference over a large spatial frequency range.

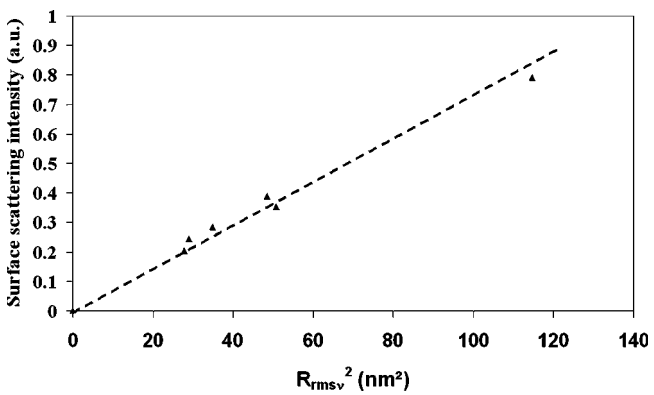

Figure 11 Surface scattering of the BMC surfaces studied (λ = 633 nm, incident angle = 20°/normal). Correlation coefficient, R^2, = 0.99.

The authors thank the Menzolit Company for its financial support.

References

1. Bartkus, E. J.; Kroekel, C. H. Appl Polym Symp 1970, 15, 113.
2. Li, W.; Lee, L. J. Polymer 2000, 41, 697.
3. Pascault, J.-P.; Sautereau, H.; Verdu, J.; Williams, R. J. J. Thermosetting Polymers; Marcel Dekker: New York, 2002.
4. Boyard, N.; Vayer, M.; Sinturel, C.; Erre, R.; Delaunay, D. J Appl Polym Sci 2004, 92, 2976.
5. Yang, Y. S.; Lee, L. J. Polymer 1988, 29, 1793.
6. Hsu, C. P.; Lee, L. J. Polymer 1991, 32, 2263.
7. Sun, B.; Yu, T. L. Macromol Chem Phys 1996, 197, 275.
8. Pattison, V. A.; Indersinn, R. R.; Schwartz, W. T. J Appl Polym Sci 1975, 19, 3045.
9. Atkins, K. E.; Koleske, J. V.; Smith, P. L.; Walter, E. R.; Matthews, V. E. 31st Annual Technical Conference, 1976.
10. Huang, Y. J.; Liang, W. C. Polymer 1996, 37, 401.
11. Li, W.; Lee, L. J. Polymer 1998, 39, 5677.
12. Suspène, L.; Fourquier, D.; Yang, Y. S. Polymer 1991, 32, 1593.
13. Boyard, N.; Vayer, M.; Sinturel, C.; Erre, R.; Levitz, P. Polymer 2005, 46, 661.
14. Huang, Y. J.; Su, C. C. Polymer 1994, 35, 2397.
15. Serré, C.; Vayer, M.; Erre, R.; Boyard, N.; Ollive, C. J Mater Sci 2001, 36, 113.
16. Huang, Y. J.; Su, C. C. J Appl Polym Sci 1995, 55, 323.
17. Li, W.; Lee, L. J. Polymer 2000, 41, 685.
18. Vayer, M.; Serré, C.; Boyard, N.; Erre, R. J Mater Sci 2002, 37, 2043.
19. Boyard, N.; Vayer, M.; Sinturel, C.; Erre, R. J Appl Polym Sci 2005, 95, 1459.
20. Cheever, D. G. J Coat Technol 1978, 50, 36.
21. Serré, C.; Vayer, M.; Erre, R.; Ollive, C. J Mater Sci 1999, 34, 4203.
22. Neitzel, M.; Blinzler, M.; Edelmann, K.; Hoecker, F. Polym Compos 2000, 21, 630.
23. Landsettle, G. A.; Jensen, J. C. 41st Annual Conference, Reinforced Plastics/Composites Institutes, Society of Plastics Industry, 1986.
24. Lucas, J. C.; Borrajo, J.; Williams, R. J. J. Polymer 1993, 34, 1886.
25. Kia, H. G. Sheet Molding Compound—Science and Technology; Hanser/Gardner Publications: Cincinnati, OH, 1993; p 257.
26. Kim, K. T.; Jeong, J. H.; Im, Y. T. J Mater Process Technol 1997, 67, 105.
27. Gorsuch, J. D.; Griffith, R. M.; Sanoki, H. Polym Plast Technol Eng 1979, 13(1), 23.
28. Mc Ewen, D. J.; Newbould, J. Polym Compos 1991, 12, 315.
29. Anonymous. Operating Manual of the Haze-Glossmeter; BYK-Gardner: Silver Spring, MD.
30. Boylan, S.; Castro, J. M. J Appl Polym Sci 2003, 90, 2557.
31. Stover, J. C. Optical Scattering: Measurement and Analysis; Fisher, R. E.; Smith, W. J., Eds.; McGraw-Hill: New York, 1990.
32. Song, J. F.; Vorburger, T. V. Surface texture; In ASM Handbook; Blau, P., Ed.; ASM Intl Publisher: Materials Park, OH, 1992; Vol. 18; pp 334–345.
33. Michel, A. Caractérisation et mesure des microgéométries de surface (Ref 1230); Techniques de l'ingénieur Ed.: Paris, 1989.
34. Deumié, C.; Richier, R.; Dumas, P.; Amra, C. Appl Opt 1996, 35, 5583.
35. Dumas, P.; Bouffakhreddine, B.; Amra, C. Europhys Lett 1993, 22, 717.
36. Deumié, C. Ph.D. Thesis, University of Aix-Marseille, France, 1997.
37. Asadchikov, V. E.; Duparré, A.; Jakobs, S.; Karabekov, A. Y.; Kozhevnikov, I. V.; Krivonosov, Y. S. Appl Opt 1999, 38, 684.
38. Duparré, A.; Kiesel, A.; Gliech, S. Rev Laser Eng 1996, 24, 220.
39. Duparré, A.; Jakobs, S. Appl Opt 1996, 35, 5052.
40. Merle; G.; Dubouloz-Monnet, F.; Grillet, C. Meas Sci Technol 2005, 16, 805.
41. Amra, C. Appl Opt 1993, 32, 5481.
42. Wolff, L. B. Opt Eng 1994, 33(1), 285.
43. Mendez, E. R.; Barrerra, R. G.; Alexander-Katz, R. Physica A 1994, 207, 137.
44. Ruppe, C.; Duparré, A. Thin Solid Films 1996, 288, 8.
45. Bennett, H. E.; Porteus, J. O. J Opt Soc Am 1961, 51(2), 123.
46. Vorburger, T. V.; Marx, E.; Lettieri, T. R. Appl Opt 1993, 32, 3401.
47. Bjuggren, M.; Krummenacher, L.; Mattson, L. Precision Eng 1997, 20(1), 33.
48. Amra, C.; Torricini, D.; Roche, P. Appl Opt 1993, 32, 5462.
49. Trezza, T. A.; Krochta, J. M. J Appl Polym Sci 2001, 79, 2221.
50. Duparré, A.; Kassam, S. Appl Opt 1993, 32, 5475.
51. Jacobs, S.; Duparré, A.; Truckenbrodt, H. Int J Match Tools Manufact 1998, 38, 733.
52. Bawolek, E. J.; Mohr, J. B.; Hirleman, E. D.; Majumdar, A. Appl Opt 1993, 32, 3377.
53. Giovannini, H.; Amra, C. Appl Opt 1998, 37(1), 103.